

A new method for cancer detection based on diffusion reflection measurements of targeted gold nanorods

Rinat Ankri
Vital Peretz
Menachem Motiei
Rachela Popovtzer
Dror Fixler

Faculty of Engineering and the
Institute of Nanotechnology and
Advanced Materials, Bar Ilan
University, Ramat Gan 52900, Israel

Abstract: This paper presents a new method for cancer detection based on diffusion reflection measurements. This method enables discrimination between cancerous and noncancerous tissues due to the intense light absorption of gold nanorods (GNRs), which are selectively targeted to squamous cell carcinoma head and neck cancer cells. Presented in this paper are tissue-like phantom and in vivo results that demonstrate the high sensitivity of diffusion reflection measurements to the absorption differences between the GNR-targeted cancerous tissue and normal, noncancerous tissue. This noninvasive and nonionizing optical detection method provides a highly sensitive, simple, and inexpensive tool for cancer detection.

Keywords: molecular imaging, nanoparticles, EGFR targeted, tissues' optical properties

Background

Nanoparticle-based contrast agents for molecular imaging became a mainstay imaging tool for selectively detecting and imaging biological processes and diseases.¹⁻³ The use of the enhanced scattering properties of gold nanoparticles as near infrared (NIR) contrast agents is under intensive study.^{4,5} This promising field builds on the safety of nonionizing radiation, ease of generation, relatively high tissue penetration depth (due to the low absorption and scattering properties), and reduced auto-fluorescence of the tissue in this spectral range.⁶ In addition, the particles' superior absorption properties have been utilized for photothermal therapy.⁶⁻⁸

Presented in this current work is a novel, noninvasive, and highly sensitive molecular cancer-detection method based on NIR diffusion reflection measurements of cancerous tissues that are targeted with gold nanorods (GNRs). The diffusion reflectance profile of an irradiated tissue depends on its absorption and scattering coefficients.^{9,10} The absorption coefficient of a tissue is predominantly determined by the concentration of the absorbance molecules, while the scattering coefficient depends mainly on the size and shape of the scattering components in the tissue, rather than their concentration.¹¹⁻¹³ Since imaging techniques that are based on scattering (with or without nanoparticles as contrast agents) suffer from relatively high background noise and low contrast, the diffusion reflection method proposes to focus mainly on the absorption properties of the targeted GNRs rather than their scattering properties. As a result, no contrast interruptions are expected.

Since GNRs have unique size- and shape-dependent optical properties, they can cause a significant change in the optical properties of the targeted tissue. Previous studies have presented diffuse reflectance measurements for cancer diagnosis¹⁴⁻¹⁶ – but without nanoparticles as contrast agents. The diffusion reflectance method described

Correspondence: Dror Fixler
Faculty of Engineering, Bar Ilan University,
Ramat Gan, 52900, Israel
Tel +972 3 5317598
Fax +972 3 7384051
Email dror.fixler@biu.ac.il

in this study presents higher efficiency and sensitivity resulting from the GNRs insertion that specifically target cancerous cells and significantly change their absorption.

In the present work, the diffusion reflectance detection method is demonstrated for head and neck cancer (HNC). The head and neck lymph nodes are located adjacent to the skin where visible-NIR light can easily penetrate. One of the major diagnosis challenges in HNC today is reliable detection of involved lymph nodes, since their status is one of the most important prognosis predictors and is also pivotal for appropriate treatment. However, assessment of lymph nodes based on currently available imaging techniques is limited in sensitivity and specificity and fails to distinguish between nonneoplastic and malignant processes. These limitations lead to the routine performance of prophylactic procedures such as extensive neck dissection and radiation. Hence, the development of more sensitive *in vivo* detection techniques is of major importance and could substantially improve HNC treatment and potential cure. In this present study, GNRs were synthesized and conjugated with anti-epidermal growth factor receptor (anti-EGFR) antibodies (Cetuximab), which home specifically to squamous cell carcinoma (SCC) HNC.¹⁷

These GNRs were intravenously injected into tumor-bearing mice. The feasibility of the diffusion reflection technique to detect cancer based on the absorption coefficient differences between cancerous and normal tissues following targeted GNRs injection was examined.

Materials and methods

The diffusion reflection method

The diffusion model^{10,18,19} is among the main approaches that best describe the light path in tissues. This approach assumes that light can be treated as a concentration of optical energy that diffuses down a concentration gradient. The loss of energy is caused by the absorbing and scattering components within the tissue.¹⁰ The diffusion model can solve several classes of image or property recovery problems. One of the most common among them is the measured $\Gamma(\rho)$. This $\Gamma(\rho)$ function, which describes the reflected light intensity (defined as Γ) at the tissue surface in several light source-detector separations (defined as ρ), presents a strong correlation to the tissue optical properties, such as the absorption coefficient μ_a and the reduced scattering coefficient μ_s' . The $\Gamma(\rho)$ function was previously described by the general formula:^{20,21}

$$\Gamma(\rho) = \frac{c_1}{(\rho)^n} \exp(-\mu\rho),$$

where c_1 is a constant, depending on the optical properties of the medium and on the sizes of the source and detector apertures; n is the power of ρ , which depends on ρ 's range and on the ratio μ_a/μ_s' and μ is the effective attenuation coefficient given by $\mu = \sqrt{3\mu_a \cdot \mu_s'}$ (for $\mu_a \ll \mu_s'$).¹⁰ As mentioned above, GNRs have unique size- and shape-dependent optical properties. They have the ability to resonantly absorb and scatter visible and NIR light upon the excitation of their surface plasmon oscillation and usually present intense and narrow absorption/scattering peaks.¹² Since the $\Gamma(\rho)$ profile highly depends on the tissue absorption and scattering properties, decorating the tumor with specifically targeted GNRs simply changes the measured $\Gamma(\rho)$ in the tumor compared with normal tissue. This phenomenon exists as long as the reflected intensity is measured at a wavelength corresponding to the GNRs absorption/scattering surface plasmon resonance peak. In the current work, tissue-like phantoms and mice were irradiated with a 650 nm laser. At this wavelength, certain sizes of GNRs can have significant absorption but a negligible scattering coefficient.¹² As a result, the measurements in this work focused on the change in tissue absorption following the GNRs injection, rather than on the change in its scattering properties which is mostly measured in NIR molecular spectroscopy and imaging techniques.

Optical setup

A noninvasive optical technique (see Figure 1) was designed and built for reflected light intensity measurements.²² The setup includes a laser diode as an excitation source (650 nm), optically bundled to a fiber (125 μm diameter) for irradiation. A portable photodiode was used as a detector, deposited at different distances, ρ , on the sample surface in order to enable $\Gamma(\rho)$ measurements. The photodiode's cross-section diameter was 1 mm^2 . The initial distance, ρ , between the light source and the first photodiode was ~ 1 mm. A micrometer plate, to which the

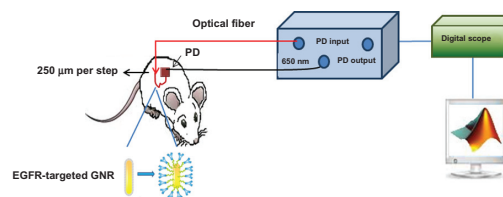


Figure 1 A schematic description of the experimental setup for the reflected light intensity measurements. Laser diode (650 nm) and an optical fiber (arrow) were used to irradiate the sample on a single point. The photodiode was in close contact with the sample surface. The micrometer plate moved in 20 incremental steps of 250 μm , enabling continuous measurements of the spatial reflectance from the sample, from 1 mm up to 6 mm from the laser diode position.

Abbreviations: EGFR, epidermal growth factor receptor; GNR, gold nanorod; PD, photodiode.

optic fiber was attached, enabled a consecutive reflected light intensity measurement. The micrometer plate was moved in 20 incremental steps of 250 μm each. The reflected light intensity was collected from different source-detector distances (ρ) varying between 1 mm (the initial distance between the light source and the photodiode) to 6 mm. The reflected intensity, $\Gamma(\rho)$ (in volts) was collected using a digital scope (Mso7034a; Agilent Technologies, Santa Clara, CA), and the data was processed using MATLAB. A schematic description of the measurement procedure is presented in Figure 1.

Nanorod fabrication and targeting

GNRs were synthesized using the seed mediated growth method.²³ Their size, shape, and uniformity were characterized using transmission electron microscopy (see Figure 2), and the resultant size was 25 nm \times 65 nm, with narrow size distribution (10%). A solution of GNRs suspended in cetyltrimethylammonium bromide (CTAB) (Sigma-Aldrich, St Louis, MO) was centrifuged at 11,000 g for 10 minutes, decanted, and resuspended in water to remove excess CTAB. To prevent aggregation, to stabilize the particles in physiological solution, and to improve blood circulation time, a layer of polyethylene glycol (mPEG-SH, molecular weight [MW] 5000 g/mol) (creative PEGWorks, Winston-Salem, NC) was adsorbed onto the GNRs. This layer also provided the chemical groups that are required for antibody conjugations (SH-PEG-COOH, MW 3400 g/mol).

The absorption spectrum of bare GNRs, PEGylated and anti-EGFR-coated GNR solutions were measured and are presented in Figure 2. Zeta potentials²⁴ (ZetaSizer 3000HS, Malvern Instruments, Worcestershire, UK) of the resulting GNRs were measured (Table 1). The zeta potential indicates the stability of colloidal dispersions, and with regards to the GNRs, the zeta potential refers to the repulsion between

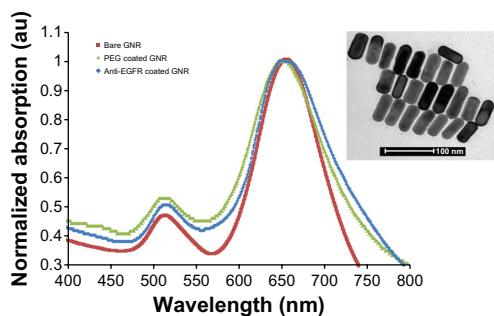


Figure 2 Ultra-violet visible absorption spectra (normalized) of bare GNRs (25 nm \times 65 nm), PEG-coated and anti-EGFR-coated GNRs, and transmission electron microscopy image of the bare GNRs (inset).

Abbreviations: EGFR, epidermal growth factor receptor; GNRs, gold nanorod; PEG, polyethylene glycol.

Table 1 Zeta potentials of bare, PEG-coated and anti-EGFR-coated GNRs

Sample	Zeta potential (mV)
Bare GNRs	+13.1
PEG-coated GNRs	+0.87
Anti-EGFR-coated GNRs	+5

Note: The zeta potentials were measured while the GNRs were suspended in water with excess CTAB.

Abbreviations: CTAB, cetyltrimethylammonium bromide; EGFR, epidermal growth factor receptor; GNR, gold nanorod; PEG, polyethylene glycol.

adjacent, similarly charged particles. GNRs stabilized in CTAB solution showed cationic surfaces (+13.1 mV). This was due to adsorbed CTAB that has a quaternary amine as a hydrophilic head. In contrast, PEG-modified GNRs showed a nearly neutral surface (+0.87 mV).

To specifically target SCC HNC, the PEGylated GNRs were coated with Cetuximab (Erbix, Merck KGaA, Germany), a monoclonal antibody against EGFRs that is highly sensitive to HNC SCC.²⁵ The binding of the EGFRs to the GNRs was confirmed by zeta potential measurement, resulting in a positive potential²⁵ (+5 mV, see Table 1). The antibody conjugated GNRs were stable for up to 3 months, confirmed by their maintenance of the same plasmon resonance.

Phantom preparation

Solid phantoms with different absorption coefficients were prepared in order to simulate skin tissues with different optical properties.²⁶ The phantoms were prepared using India ink 0.1% as an absorbing component, Intralipid® 20% (Lipofundin MCT/LCT 20%, B. Braun Melsungen AG, Melsungen, Germany) as a scattering component,²⁷ and 1% agarose powder (SeaKem LE Agarose, Lonza, Norwalk, CT) in order to convert the solution into a gel. The solutions were heated and mixed (at a mixing temperature of $\sim 90^\circ\text{C}$) while the agarose powder was slowly added. The absorption spectrum of the India ink was determined using a spectrophotometer, and the absorption coefficient of each phantom was calculated according to the concentration of the ink in each solution. The scattering properties of the phantoms were determined according to the scattering coefficients presented by Cubeddu et al.²⁷ The phantoms were prepared in cell culture plates (90 mm) and were cooled under vacuum conditions (to avoid bubbles). Five phantoms with the same scattering properties and different absorption coefficients were prepared. Each phantom contained 2% of Intralipid and increasing concentrations of India ink: 5.0×10^{-4} , 2.5×10^{-3} , 5.0×10^{-3} , 7.0×10^{-3} , and 1.0×10^{-1} (%). The resulted scattering coefficient was $\sim 1.6 \text{ mm}^{-1}$, and the resulting absorption

coefficients were $\mu_a = 0.0064, 0.0126, 0.0180, 0.0227,$ and 0.0295 mm^{-1} , respectively.

GNRs (10 mg/mL) were added into two identical phantom solutions, containing $2 \times 10^{-3}\%$ of ink and 2% of Intralipid (optical properties of $\mu_a = 0.0115 \text{ mm}^{-1}$ and $\mu_s = 1.6 \text{ mm}^{-1}$) to achieve final concentrations of 0.03 and 0.008 mg/mL of gold in the phantoms. The solutions were heated and mixed at a temperature of approximately 90°C while the agarose powder was slowly added. Then, the phantom solutions were poured into a 24-well plate (each well with a 16 mm diameter) and were cooled under vacuum conditions.

In vitro experiment

A-431 cells (2.5×10^6) in 5 mL Dulbecco's modified Eagle's medium containing 5% fetal calf serum, 0.5% penicillin, and 0.5% glutamine were divided into two groups for a quantitative cell binding study (each experimental group was run in triplicate). The first group was incubated with 50 μL of anti-EGFR-coated GNRs (25 mg/mL) for 30 minutes at 37°C , and the second group (negative control) was incubated under the exact same conditions with anti-rabbit immunoglobulin G (IgG)-coated GNRs. After incubation, the medium was washed twice with phosphate buffered saline followed by the addition of 1 mL of aqua regia $\text{HCl}:\text{HNO}_3$ (1:3) (Sigma-Aldrich). After evaporation of the acid, the sediment was dissolved in 5 mL 0.05 M HCl. The gold concentrations of the samples were quantified by atomic absorption spectroscopy (AA 140; Agilent Technologies, Santa Clara, CA).

In vivo experiment

This new method for tumor detection was evaluated using mice bearing human HNC derived from an A-431 SCC cell line. A-431 cells (2×10^6) were injected subcutaneously

into the back flank area of 10–11-week-old nude mice. These cells express from 2×10^4 to 2×10^6 EGFRs per cell.^{28,29} When the tumor reached a size of 7–9 mm in diameter, the mice received 100 μL (25 mg/mL) of immuno-targeted GNRs by tail vein injection. Mice tumor and normal tissue (control #1; identical organ on the opposite side, without tumor, after the GNRs injection) were scanned immediately after GNRs injection and up to 10 hours post-injection. As a control experiment, the same mice were scanned (tumor and normal tissues) before GNRs injection (control #2 and #3, respectively). Diffusion reflection measurements were performed on all samples to test the ability to specifically and sensitively detect tumors.

All in vivo measurements were performed under appropriate anesthesia: the mice barrier-controlled facility was under the strict care of the veterinarian in charge of the Institutional Animal Care and Use Committee (IACUC). The mice were inspected daily by the veterinarian, who handles the appropriate tests and treatment protocols, as required. All research protocols were followed closely by the veterinarian. All major procedures were performed in the surgical facilities using general anesthesia and standard, aseptic surgical techniques.

Results

Phantom results

The reflected light intensity from five different phantoms was measured using the experimental setup described above. Representative results of the reflected light intensity profiles are presented in Figure 3A. The experimental results correlate well with the analytical predictions of the diffusion theory: the larger the μ_a , the sharper the graph's slope. The phantoms' absorption coefficients were 0.0064, 0.0126, 0.0180, 0.0227, and 0.0295 mm^{-1} .

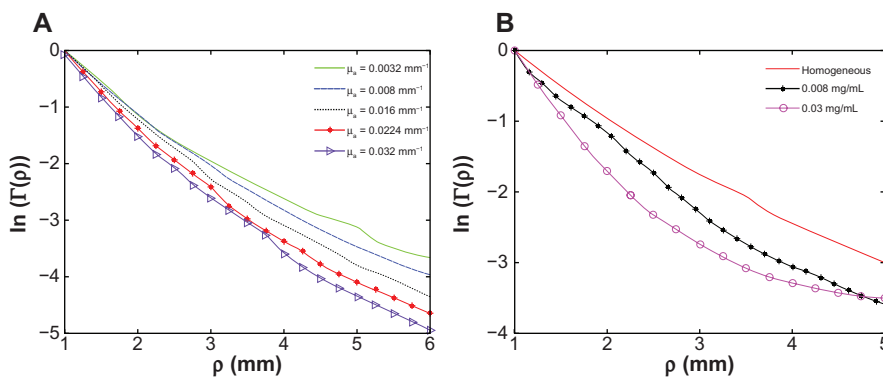


Figure 3 Diffusion reflection intensity (in semi-logarithmic scale) as a function of the distance between the detector and the light source, for different phantoms as follows: **(A)** homogeneous phantoms with the same reduced scattering property $\mu_s' = 1.6 \text{ mm}^{-1}$ but different absorption coefficients of 0.0064, 0.0126, 0.0180, 0.0227, and 0.0295 mm^{-1} (the solid, dashed, dotted, diamond marked, and triangle marked lines, respectively); and **(B)** a homogeneous phantom (the solid line) and phantoms with gold nanorod particles of different concentrations (the cross- and the circle-marked lines).

0.0180, 0.0227, and 0.0295 mm^{-1} , and the slopes represent increasing respective negative values of: 0.57, 0.64, 0.69, 0.74, and 0.81. The increasing negative values of the slopes directly correlate with the increasing concentrations of ink in the phantoms. These results indicate the experimental setup's ability to clearly distinguish between different absorption coefficients.

Figure 3B presents the reflected light intensity from three solid phantoms as follows: one homogeneous phantom (a solid phantom without GNRs, $\mu_a = 0.0115 \text{ mm}^{-1}$ and $\mu_s' = 1.6 \text{ mm}^{-1}$) and two phantoms containing 0.008 and 0.030 mg/mL of GNRs. The results clearly indicate that the presence of GNRs within the phantom increases the slope of the reflected intensity profile. Moreover, the higher the GNRs concentration, the sharper the reflectance graph slope. The phantom with 0.008 mg/mL of GNRs represents a negative slope of 1.11, while the phantom containing 0.030 mg/mL of GNRs represents a negative slope of 1.39. As mentioned above, the GNRs have high absorption at 650 nm but negligible scattering properties. Therefore, the observed increase in the graph's slope is due to the increase in the absorption of the irradiated phantom resulting from the presence of the GNRs.

In vitro cell-binding experiment

To evaluate the specificity of the interaction between the antibody-coated GNRs and the A-431 SCC cancer cells (which highly express the EGFR), two types of GNRs were introduced to the cells: the first was specifically coated with anti-EGFR antibody; whilst the second, which was used as a negative control, was coated with a nonspecific antibody (anti-rabbit IgG). Flame atomic absorption spectroscopy measurements quantitatively demonstrated that the active tumor targeting (anti-EGFR-coated GNRs) was significantly more specific than the control experiment (anti-rabbit IgG-coated GNRs). The A-431 cells took up $21.8 \pm 2.3 \mu\text{g}$ of targeted GNRs, whilst parallel cells in the negative control experiment absorbed only $0.20 \pm 0.01 \mu\text{g}$ of GNRs.²⁵ These results correlate well with previously published studies, which report that head and neck SCC express from 2×10^4 to 2×10^6 EGFRs per cell.^{28,29}

In vivo results

The tumor-bearing mice were irradiated, under appropriate anesthesia, and the reflected light intensity was measured using the optical setup described above. The reflectance measurements were performed before the GNRs injection and for several delay times (15 minutes, 3, 5, and >10 hours)

post-injection. The slopes of the reflected light intensity profiles were calculated, and average results are shown in Figure 4.

Figure 4 compares the reflected light intensity slopes (absolute values) of the cancerous and the normal tissues, for three representative times: (1) before GNRs injection (control #2 and #3), (2) immediately (~15 minutes) after intravenous injection, and (3) more than 10 hours post-injection. It is clearly demonstrated that >10 hours post GNRs injection there is a significant change (of more than 60%) between the reflectance profiles of the cancerous and the normal tissue (control #1). This change results from specific accumulation of GNRs in the tumor. It is also demonstrated that immediately after GNRs injection, as well as for the delay times of 3 and 5 hours post-injection (results not shown), the reflectance profiles of both the cancerous and the normal tissues present an increase in their slopes, which indicates the GNRs' long circulating time in the blood. After that time, the GNRs were gradually cleared from the blood until their complete clearance from the normal tissue, resulting in a decrease of its reflectance slope compared with the cancerous tissue, which kept a stable value of 0.8. Regarding control #3 (normal tissue before the GNRs injection), the mice's normal tissues were irradiated in different areas in the mice's skin tissue, and the reflectance slopes of the different areas were almost identical, resulting in a small standard deviation (small error bar in the left column in Figure 4). This high similarity of these slopes indicates that any area of the skin can be irradiated, and the resulted reflection slope will always be lower than the tumor reflection slope 10 hours post the GNRs injection, enabling a consistent tumor detection.

Figure 5 emphasizes the difference between the slopes before GNRs injection and >10 hours post-injection for the

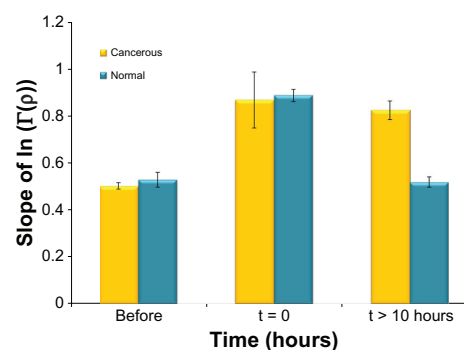


Figure 4 Comparison between the reflected light intensity slopes (absolute values) of the cancerous and normal tissues at several time points.

Notes: The results are the average of five to ten diffusion reflection measurements of different mice. The error bars represent error of the mean. The highest error bar is of the normal tissue immediately post injection, indicating different rates of the gold nanorod flow in the different mice's blood.

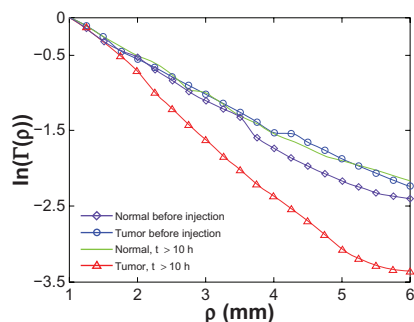


Figure 5 Diffusion reflection intensity (in semilogarithmic scale) as a function of the distance between the detector and the light source. The graph emphasizes the difference between the slopes before GNRs injection and >10 hours post-injection for the cancerous and normal tissues. While the absorption value and the reflectance slope of the normal tissue is the same before GNRs insertion and more than 10 hours post-injection, the tumor clearly presents a higher absorption value resulting in a sharper slope.

Abbreviation: GNRs, gold nanorods.

cancerous and normal tissues, as directly obtained from the reflected light intensity measurements. While the reflectance slope, which directly indicates the absorption coefficient of the normal tissue, is the same before GNRs insertion and >10 hours post-injection, the tumor clearly represents a sharper slope. This clear discrimination between cancerous and normal tissue enables sensitive and specific cancer detection based on diffusion reflection measurements.

Discussion

This work presents a novel in vivo cancer detection technique that utilizes the unique favorable absorption properties of GNRs in the NIR region. The ability to specifically deliver and target high concentrations of GNRs exclusively to the tumor significantly elevated the absorption coefficient of the tumor and enabled the discrimination (by more than 60%) between cancerous and noncancerous tissues. As opposed to NIR imaging techniques that utilize the scattering properties of the tissue, the key advantage of the proposed diffusion reflection technique is its ability to directly correlate between the absorbers' molecules concentration and the $\Gamma(\rho)$ signal. Further investigation is required to best correlate between the diffusion reflection slope and the GNRs concentration in the tissue, which can indicate the tumor size. This noninvasive and nonionizing optical detection method is expected to provide a highly sensitive, simple, and inexpensive tool for cancer detection.

Conclusion

A novel and simple method for cancer detection is presented. Using the absorption properties of gold nanoparticles, the detection of HNC was enabled based on diffusion reflection measurements of the cancerous tissue.

Acknowledgments

This work was supported by Merck Sorono, the Elias, Genevieve and Geogianna Atol Charitable Trust, and the Katz Family Grant Incentive Program.

Disclosure

The authors report no conflicts of interest in this work.

References

- Lee JH, Huh YM, Jun YW, et al. Artificially engineered magnetic nanoparticles for ultra-sensitive molecular imaging. *Nat Med*. 2007;13:95–99.
- Weissleder R, Pittet MJ. Imaging in the era of molecular oncology. *Nature*. 2008;452:580–589.
- Hilderbrand SA, Weissleder R. Near-infrared fluorescence: application to in vivo molecular imaging. *Curr Opin Chem Biol*. 2010;14:71–79.
- Chen J, Saeki F, Wiley BJ, et al. Gold nanocages: bioconjugation and their potential use as optical imaging contrast agents. *Nano Lett*. 2005;5:473–477.
- Gobin AM, Lee MH, Halas NJ, James WD, Drezek RA, West JL. Near-infrared resonant nanoshells for combined optical imaging and photothermal cancer therapy. *Nano Lett*. 2007;7:1929–1934.
- Huang X, El-Sayed IH, Qian W, El-Sayed AM. Cancer cell imaging and photothermal therapy in the near-infrared region by using gold nanorods. *J Am Chem Soc*. 2006;128:2115–2120.
- Lowery AR, Gobin AM, Day ES, Halas NJ, West JL. Immunonanoshells for targeted photothermal ablation of tumor cells. *Int J Nanomedicine*. 2006;1:149–154.
- Lal S, Clare SE, Halas NJ. Nanoshell-enabled photothermal cancer therapy: impending clinical impact. *Acc Chem Res*. 2008;41:1842–1851.
- Reif R, A'Amar O, Bigio IJ. Analytical model of light reflectance for extraction of the optical properties in small volumes of turbid media. *Appl Opt*. 2007;46:7317–7328.
- Jacques ST, Pogue BW. Tutorial on diffuse light transport. *J Biomed Opt*. 2008;13:0413021–0413019.
- Lee KS, El-Sayed MA. Dependence of the enhanced optical scattering efficiency relative to that of absorption for gold metal nanorods on aspect ratio, size, end-cap shape, and medium refractive index. *J Phys Chem B*. 2005;109:20331–20338.
- Jain PK, Lee KS, El-Sayed IH, El-Sayed MA. Calculated absorption and scattering properties of gold nanoparticles of different size, shape, and composition: applications in biological imaging and biomedicine. *J Phys Chem B*. 2006;110:7238–7248.
- Shimada M, Sato C, Hoshi Y, Yamada Y. Estimation of the absorption coefficients of two-layered media by a simple method using spatially and time-resolved reflectances. *Phys Med Biol*. 2009;54:5057–5071.
- Yang Y, Celmer EJ, Koutcher JA, Alfano RR. UV reflectance spectroscopy probes DNA and protein changes in human breast tissues. *J Clin Laser Med Surg*. 2001;19:35–39.
- Bigio IJ, Bown SG, Briggs G, et al. Diagnosis of breast cancer using elastic-scattering spectroscopy: preliminary clinical results. *J Biomed Opt*. 2000;5:221–228.
- Zhu C, Palmer GM, Breslin TM, Harter J, Ramanujam N. Diagnosis of breast cancer using diffuse reflectance spectroscopy: comparison of a Monte Carlo versus partial least squares analysis based feature extraction technique. *Las Surg Med*. 2006;38:714–724.
- Baselga J. The EGFR as a target for anticancer therapy – focus on cetuximab. *Eur J Cancer*. 2001;37:16–22.
- Das M, Xu C, Zhu Q. Analytical solution for light propagation in a two-layer tissue structure with a tilted interface for breast imaging. *Appl Opt*. 2006;45:5027–5036.
- Johnson PM, Faez S, Legendijk AD. Full characterization of anisotropic diffuse light. *Opt Exp*. 2008;16:7435–7446.

20. Schmitt JM, Zhou GX, Walker EC, Wall RT. Multi layer model of photon diffusion in skin. *J Opt Soc Am A*. 1990;7:2141–2153.
21. Farrell TJ, Patterson MS, Wilson B. A diffusion theory model of spatially resolved, steady-state diffuse reflectance for the noninvasive determination of tissue optical properties in vivo. *Med Phys*. 1992;19:879–888.
22. Ankri R, Taitelbaum H, Fixler D. Reflected light intensity profile of two-layer tissues – phantom experiments. *J Biomed Opt*. 2011;16(8):085001.
23. Nikoobakht B, El-Sayed MA. Preparation and growth mechanism of gold nanorods (NRs) using seed-mediated growth method. *Chem Mater*. 2003;15:1957–1962.
24. Maldiney T, Richard C, Seguin J, Wattier N, Bessodes M, Scherman D. Effect of Core Diameter, Surface Coating, and PEG chain length on the biodistribution of persistent luminescence nanoparticles in mice. *ACS Nano*. 2011;5:854–862.
25. Reuveni T, Motiei M, Romman Z, Popovtzer A, Popovtzer R. Targeted gold nanoparticles enable molecular CT imaging of cancer: an in vivo study. *Int J Nanomedicine*. 2011;6:2859–2864.
26. Dam JS, Pedersen CB, Dalgaard T, Fabricius PE, Aruna P, Andersson-Engels S. Fiber-optic probe for noninvasive real-time determination of tissue optical properties at multiple wavelengths. *Appl Opt*. 2001;40:1155–1164.
27. Cubeddu R, Pifferi A, Taroni P, Torricelli A, Valentini G. A solid tissue phantom for photon migration studies. *Phys Med Biol*. 1997;42:1971–1979.
28. Stanton P, Richards S, Reeves J, et al. Epidermal growth factor receptor expression by human squamous cell carcinomas of the head and neck, cell lines and xenografts. *Br J Cancer*. 1994;70:427–433.
29. Todd R, Wong DT. Epidermal growth factor receptor (EGFR) biology and human oral cancer. *Histol Histopathol*. 1999;14:491–500.

International Journal of Nanomedicine

Publish your work in this journal

The International Journal of Nanomedicine is an international, peer-reviewed journal focusing on the application of nanotechnology in diagnostics, therapeutics, and drug delivery systems throughout the biomedical field. This journal is indexed on PubMed Central, MedLine, CAS, SciSearch®, Current Contents®/Clinical Medicine,

Submit your manuscript here: <http://www.dovepress.com/international-journal-of-nanomedicine-journal>

Dovepress

Journal Citation Reports/Science Edition, EMBase, Scopus and the Elsevier Bibliographic databases. The manuscript management system is completely online and includes a very quick and fair peer-review system, which is all easy to use. Visit <http://www.dovepress.com/testimonials.php> to read real quotes from published authors.